The Journal of Chemical Physics ARTICLE scitation.org/journal/jcp

Characterization of the ultrafast spectral diffusion and vibronic coherence of TIPS-pentacene using 2D electronic spectroscopy

Cite as: J. Chem. Phys. 155, 014302 (2021); doi: 10.1063/5.0055528
Submitted: 30 April 2021 • Accepted: 7 June 2021 •
Published Online: 1 July 2021

Duc Viet Le,[1] Jessica M. de la Perrelle,[2] Thanh Nhut Do,[1] Xuan Leng,[1,a)] Patrick C. Tapping,[2] Gregory D. Scholes,[3] Tak W. Kee,[2,b)] and Howe-Siang Tan[1,b)]

AFFILIATIONS

[1] Division of Chemistry and Biological Chemistry, School of Physical and Mathematical Sciences, Nanyang Technological University, 21 Nanyang Link, Singapore 637371
[2] Department of Chemistry, University of Adelaide, Adelaide SA 5005, Australia
[3] Department of Chemistry, Princeton University, Princeton, New Jersey 08544, USA

Note: This paper is part of the JCP Special Topic on Coherent Multidimensional Spectroscopy.
[a)] **Present Address:** Department of Physics, School of Physical Science and Technology, Ningbo University, Ningbo 315211, China.
[b)] **Authors to whom correspondence should be addressed:** tak.kee@adeleide.edu.au and howesiang@ntu.edu.sg

ABSTRACT

TIPS-pentacene is a small-molecule organic semiconductor that is widely used in optoelectronic devices. It has been studied intensely owing to its ability to undergo singlet fission. In this study, we aim to develop further understanding of the coupling between the electronic and nuclear degrees of freedom of TIPS-pentacene (TIPS-Pn). We measured and analyzed the 2D electronic spectra of TIPS-Pn in solutions. Using center line slope (CLS) analysis, we characterized the frequency-fluctuation correlation function of the 0–0 vibronic transition. Strong oscillations in the CLS values were observed for up to 5 ps with a frequency of 264 cm^{-1}, which are attributable to a large vibronic coupling with the TIPS-Pn ring-breathing vibrational mode. In addition, detailed analysis of the CLS values allowed us to retrieve two spectral diffusion lifetimes, which are attributed to the inertial and diffusive dynamics of solvent molecules. Amplitude beating analysis also uncovered couplings with another vibrational mode at 1173 cm^{-1}. The experimental results can be described using the displaced harmonic oscillator model. By comparing the CLS values of the simulated data with the experimental CLS values, we estimated a Huang–Rhys factor of 0.1 for the ring-breathing vibrational mode. The results demonstrated how CLS analysis can be a useful method for characterizing the strength of vibronic coupling.

INTRODUCTION

Two-dimensional electronic spectroscopy (2DES) has contributed much to the understanding of the structural and dynamic characteristics of a variety of systems, including light harvesting complexes, solid state materials, and nano-structured solar cells.[1–3] 2DES experiments measure frequency-resolved heterodyne signals of the stimulated photon echo and belong to the family of third-order nonlinear optical spectroscopic methods. A typical 2DES experiment consists of three ultrafast laser pulses. The first two pulses resonate with the excitation gap of the system, and the third pulse probes the evolution of the excited population over time.[4] By Fourier transforming the coherence time, which is the time separation between the first and second pulses, we can obtain an additional frequency dimension associated with pump or excitation frequencies. The additional dimension allows 2D electronic spectra to express a wealth of information that is often unavailable from conventional transient absorption spectroscopy. Complex physical and chemical processes involving multiple states in the system, such as energy transfer,[5,6] relaxation of different high-energy states,[7–9] coherence between multiple states,[10,11] and system-environment interactions,[12,13] can be studied. In particular, due to the presence of the diagonal and off-diagonal peaks, 2D electronic spectra offer insights into the behavior of excitonic levels,

as well as the interactions between different energy states. The dynamics of the diagonal and off-diagonal peaks offers significant information regarding how different energy states couple with each other and how one energy state behaves under experimental conditions.[14,15]

In addition, the effects of the surrounding environment can be understood from the 2D peak shape of the excited state. The 2D peak shape can inform the dynamics of the system at the molecular level.[16,17] Multiple studies dedicated to this subject have provided both qualitative explanations and mathematical descriptions of how the 2D peak shape is related to the dynamics of the system and how this information can be extracted from a 2D electronic spectrum.[18,19] One way the interaction between the solvent and a molecule can be quantified is through the frequency-fluctuation correlation function (FFCF), $C_{ii}(t) = \langle \delta\omega_i(t)\delta\omega_i(0)\rangle$. The FFCF represents the ensemble average of how the frequency of a transition fluctuates with time. It is a sensitive measure of the strength of the interaction between the molecule and its surrounding environment.[20,21] Nonlinear optical techniques, such as three-pulse photon echo peak shift spectroscopy, have been used to characterize the FFCF.[22,23] However, the larger dataset measured by 2DES allows for higher sensitivity and hence better precision when extracting the FFCF. There are several methods to capture the system-environment dynamics from a 2D electronic spectrum.[24] One analysis method that is commonly used is the center line slope (CLS) analysis.[25,26] CLS analysis of spectral diffusion has been performed on several systems, such as photosynthetic pigments,[27,28] quantum dots,[29] biological molecules,[30] and reverse micelles,[31] which provided crucial information regarding how the environment interacts with these systems and affects their spectroscopic properties. Apart from the FFCF decay, coherent modulations of the transition can also be tracked using CLS analysis. For example, if the transition is coupled to a harmonic oscillator, the resultant CLS is shown to oscillate along the waiting time (T_w). In 2DES, this phenomenon was first observed by Nemeth *et al.* in the dye molecule PERY in toluene.[32] Further examples of such CLS beating were reported by Šanda *et al.*[33]

CLS analysis on molecular chromophores, including 6,13-bis(triisopropylsilylethynyl) pentacene (TIPS-Pn), can offer insight into the coupling between the electronic and vibrational degrees of freedom. TIPS-Pn is a widely used organic semiconducting material that is intensely studied in the field of singlet fission (SF),[34] an exciton multiplication process that is of interest due to its potential to increase the efficiency of photovoltaic cells.[35] During SF, a molecule in a singlet excited state couples to a neighboring ground-state molecule, resulting in both molecules occupying a lower energy triplet state, as described below.[36,37] The process occurs via the triplet pair intermediate, ^{1}(TT), in which the two triplets are strongly coupled, resulting in an overall singlet character,

$$S_1 + S_0 \rightleftharpoons {}^1(TT) \rightleftharpoons T_1 + T_1.$$

Recently, broadband pump–probe and 2DES studies have reported that vibronic states may be involved in SF in crystalline TIPS-Pn.[38,39] However, 2DES is yet to be used to investigate the coherence of the singlet states of TIPS-Pn in the absence of SF. Here, we focus on TIPS-Pn in solutions, whereby SF is inaccessible due to a sufficiently low concentration.[40]

In this study, 2DES measurements were performed on TIPS-Pn in dilute solutions. CLS analysis revealed spectral diffusion dynamics in the diagonal peak arising from the solvent relaxation dynamics of TIPS-Pn. The 2DES measurements also exhibit strong beating in the CLS. Although oscillations in CLS values have been reported before,[32,33,41,42] we present here experimental CLS oscillation signals that are strong enough for clear analysis. We can use a displaced harmonic oscillator model to quantitatively explain the dynamics observed in the CLS analysis. The more conventional amplitude beating data characterized using 2D Fourier maps are shown to be consistent with the CLS analysis. The experimental analysis and simulation are discussed, with focus on the vibronic coupling between vibrational and electronic degree of freedoms.

EXPERIMENTAL METHODS

Powdered 6,13-bis(triisopropylsilylethynyl)pentacene (TIPS-Pn) was dissolved in toluene or freshly distilled tetrahydrofuran (THF) to form a solution with the optical density of 0.25 OD (toluene) or 0.70 OD (THF) at 15 500 cm^{-1} (corresponding to the 0–0 transition) in a 1-mm quartz cuvette. The absorption spectrum of TIPS-Pn in toluene is shown in Fig. 1 and that in THF is presented in Fig. S3 in the supplementary material.

2DES measurements were performed using two setups. Setup I consisted of a femtosecond laser system with a partially collinear pump–probe beam geometry.[43,44] Supercontinuum light was created by focusing 1.8 W of the 800-nm output from a Ti:Sapphire regenerative amplifier (Legend Elite, Coherent) into a home-built 1.2-m tube pressurized with 2.2 bars of argon gas. The resulting supercontinuum from the optical filamentation process was split by a UV-fused silica wedge window into two beams, which served as the pump and probe pulses. The pump pulse was compressed by a chirped mirror pair (DCM10, Laser Quantum) and then shaped by an acousto-optic programmable pulse shaper (Dazzler, Fastlite) into a phase-locked double pulse train. The interpulse delay time t_1

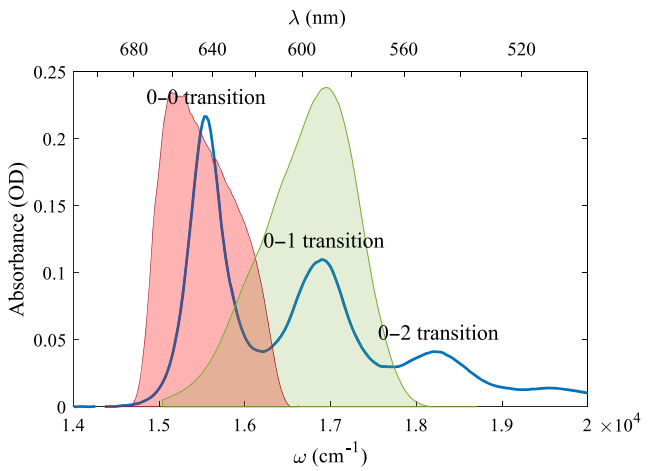

FIG. 1. Absorption spectrum of TIPS-Pn in toluene and the excitation spectra used in setup I (red) and setup II (green).

between the two pump pulses was scanned from 0 to 100 fs with 4-fs steps by the pulse shaper. The probe pulse was compressed by a similar chirped mirror pair. The cross-correlation between the pump and probe pulses was measured in neat toluene, which gave a full-width at half-maximum (FWHM) of 60 fs. The waiting time T_w was controlled by a retroreflector attached on a motorized delay stage and scanned from −300 fs to 5 ps with 20 fs time steps. The t_1-dependent transient absorption signal $S(t_1, T_w, \omega_3)$ was resolved by utilizing a 1 × 2 phase cycling scheme with a partial rotating frame of reference, and numerical discrete Fourier transformation was carried out over t_1 to obtain the final 2D electronic spectra $S(\omega_1, T_w, \omega_3)$. In setup I, the pump spectrum was centered at 15 500 cm^{-1} (645 nm), matching the first vibronic transition energy of the TIPS-Pn molecule (red spectrum in Fig. 1).

Setup II was based on a non-collinear BOXCARS geometry and was described previously.[45] The 100-fs output from a Ti:Sapphire regenerative amplifier (Spitfire Pro XP 100F, Spectra-Physics) was directed to a non-collinear optical parametric amplifier pumped at 400 nm, producing broadband pulses centered at 600 nm with a FWHM bandwidth of 66 nm. The pulses were compressed by a single-grating and single-prism compressor to 12-fs FWHM duration. The compressed pulses were split into four beams by a diffractive optic and collimated by a concave mirror into the BOXCARS geometry. Two of the beams, k_1 and k_2, were individually passed through a pair of rotating optical flats, which served as the delay lines for t_1 and T_w. The third beam, k_3, was passed through a glass flat providing a constant time delay, and the fourth beam was passed through a 4 OD neutral density filter and used as a local oscillator (LO). The four beams were focused on the sample by another concave mirror. The third-order signal was emitted collinearly with the LO and detected by an imaging spectrograph and camera (Shamrock SR303-I and Newton 970, Andor). To collect data in the nonrephasing and rephasing phase-matching directions, t_1 was scanned from −45 to 45 fs such that k_1 and k_2 were swapped when the sign of t_1 was swapped. The ω_1 axis was generated by Fourier transform over t_1, the ω_3 axis was generated by heterodyne detection, and T_w was scanned from 0 to 500 fs. The excitation pulse for setup II was broad and able to cover the first and second vibronic transitions of TIPS-Pn (green spectrum in Fig. 1).

Setup I, which scanned the waiting time up to hundreds of ps, yielded ps timescale spectral diffusion and the lower frequency vibrational dynamics. Setup II, which had a higher time resolution and a wider excitation spectral bandwidth, had a more limited T_w range. The BOXCARS of setup II allowed access to the nonrephasing and rephasing data. This setup was used to measure the dynamics and "w_1- and w_3-dependence" the higher frequency modes.

THEORY

In the time-dependent perturbation theory framework that is commonly used to describe nonlinear optical spectroscopy,[46] such as 2DES, the nonlinear optical response functions are summarized by enumerating the various coherence transfer pathways, which are represented graphically by double-sided Feynman diagrams (DSFDs). These diagrams describe the 2DES spectral peaks and can be expressed as the following third-order nonlinear optical response functions:

$$R_1(t_1, T_w, t_3) = \exp[-i\omega_{eg}(t_3 + t_1)] \exp\big[-g(t_1) - g^*(t_3) - g^*(T_w) + g(t_1 + T_w) + g^*(t_3 + T_w) - g(t_1 + t_3 + T_w)\big], \tag{1}$$

$$R_2(t_1, T_w, t_3) = \exp[-i\omega_{eg}(t_3 - t_1)] \exp\big[-g^*(t_1) - g^*(t_3) + g(T_w) - g^*(t_1 + T_w) - g(t_3 + T_w) + g^*(t_1 + t_3 + T_w)\big], \tag{2}$$

$$R_3(t_1, T_w, t_3) = \exp[-i\omega_{eg}(t_3 - t_1)] \exp\big[-g^*(t_1) - g(t_3) + g^*(T_w) - g^*(t_1 + T_w) - g^*(t_3 + T_w) + g^*(t_1 + t_3 + T_w)\big], \tag{3}$$

$$R_4(t_1, T_w, t_3) = \exp[-i\omega_{eg}(t_3 + t_1)] \exp\big[-g(t_1) - g(t_3) - g(T_w) + g(t_1 + T_w) + g(t_3 + T_w) - g(t_1 + t_3 + T_w)\big], \tag{4}$$

where $g(t)$ is the lineshape function and $g^*(t)$ is the complex conjugated form of the lineshape function. In this system, we used a complex function to describe $g(t)$; therefore, its complex conjugated form is involved in the equations. ω_{eg} is the energy difference in the two-level system, t_1 is the time separation between the first and the second interaction, and t_3 is the time between the third interaction and detection of the signal.

A common way to model the lineshape function is to use a system-bath model in which a two-level system is coupled to a series of Brownian oscillators. In this system, we simulated the 2D electronic spectra by separating the Brownian oscillators into two parts. The first part is a summation of overdamped harmonic oscillators, representing the effects of an environmental bath labeled $g_b(t)$, and the second part describes a single underdamped harmonic oscillator, denoted as $g_v(t)$, which usually arises from coupling with a specific vibrational mode of the molecule. The lineshape function is thus described as

$$g(t) = g_b(t) + g_v(t). \tag{5}$$

Details of the derivation of $g_b(t)$ and $g_v(t)$ can be found in the supplementary material (Sec. 1). The formula of the environmental bath used in the simulation is

$$g_b(t) = \frac{t}{T_2} + \sum_k \frac{\Delta_k^2}{\gamma_k^2}[\exp(-\gamma_k t) + \gamma_k t - 1], \tag{6}$$

in which T_2 is the homogeneous dephasing time. A summation over k components is used to represent the remaining bath interactions that arise from different solvent chromophore interactions over different timescales.[27,47] For each component k, Δ_k is the fluctuation amplitude and γ_k is the inverse correlation time.

The expression for the underdamped harmonic oscillator is

$$g_v(t) = -i\lambda_v t + S_v\left[\Xi(T) - \exp(-\gamma_v t)\left(\frac{\Xi(T) - 1}{2}\exp(i\omega_v t) + \frac{\Xi(T) + 1}{2}\exp(-i\omega_v t)\right)\right], \tag{7}$$

with $\Xi(T) = \coth\left(\frac{\hbar\omega_v}{2kT}\right)$ and $S_v = \frac{\lambda_v}{\omega_v}$ is the Huang–Rhys factor that represents the strength of the vibronic coupling between electronic and vibrational degree of freedom. λ_v is the reorganization energy, γ_v is the damping rate, and ω_v is the frequency of the vibrational mode.

RESULTS

Figure 1 shows the absorption spectrum of TIPS-Pn in toluene. The peak with the highest intensity at 15 500 cm^{-1} belongs to the transition between the ground vibrational state of the first and second electronic states of the molecule (denoted as 0–0 transition). The other peaks at 16 800 and 18 200 cm^{-1} are the vibronic transitions from the ground vibrational state of the first electronic state to the first (denoted as 0–1 transition) and the second vibrational states (denoted as 0–2 transition) in the second electronic state, respectively. In this study, we used setup I to excite TIPS-Pn at the first vibronic transition and observed the 2D electronic spectra at the probe window of 14 500–16 800 cm^{-1}. We further used the displaced harmonic oscillator model mentioned in the Theory section to simulate the CLSω_3. We used setup II to excite the molecule at both the first and the second vibronic transitions and probe the dynamics between 15 000 and 17 000 cm^{-1}. To understand the effect vibrational modes have in the 2D electronic spectrum, we measured the Raman spectrum of TIPS-Pn and assigned the modes using DFT/B3LYP at 6-31G(d, p) calculations. The results are listed in the supplementary material (Sec. 6).

Excitation of the 0–0 transition (setup I)

In Fig. 2, we show the 2D electronic spectra of TIPS-Pn at T_w = 0.1 ps and 3 ps measured using setup I. The amplitude of the peak results from the ground state bleach (GSB) and stimulated emission (SE). The peak shape shows a clear transition from a diagonally elongated shape to a more symmetric shape after 3 ps with intense oscillations over T_w.

To quantify the observed behavior in the peak shape of the 0–0 vibronic diagonal peak, we performed CLSω_3 analysis, which yielded the center lines shown as red lines in Fig. 2 (details about the analysis can be found in Sec. 2 of the supplementary material). The resultant CLSω_3 vs T_w dynamics are represented in Fig. 3(a).

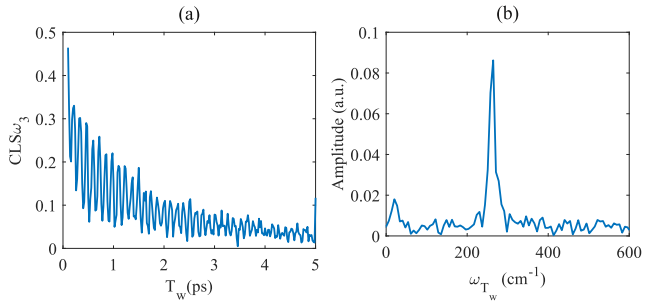

FIG. 3. (a) CLSω_3 as a function of T_w obtained from the CLS analysis of 2D electronic spectra shown in Fig. 2 and (b) the corresponding Fourier transformed result.

The CLSω_3 decays on a timescale of ~2 ps and has a prominent oscillatory feature with a period of ~120 fs, corresponding to a frequency of 264 ± 8 cm^{-1} [estimated FWHM from Fig. 3(b)]. From published data of toluene,[48,49] we can rule out the possibility that this frequency arises from the solvent, while it matches the ring-breathing mode of the pentacene molecule (Fig. S7a).[50] The 2D electronic spectrum can also be subjected to an amplitude beating analysis.[51–53] Kinetic traces near the diagonal and anti-diagonal regions are taken as comparison and shown in Fig. 4. The traces exhibit a strong oscillatory feature with the same frequency as the CLS. The oscillatory phases of the traces are different, in which the diagonal traces oscillate out-of-phase with the anti-diagonal traces [Fig. 4(b)].

To better visualize the distribution of amplitude beating over the whole 2D spectrum of the 0–0 vibronic diagonal peak, we performed a Fourier transform of the beating residue extracted from the 2DES along T_w to obtain the 2D Fourier maps. The detailed workflow is depicted in the supplementary material (Sec. 3). Figure 5(a) shows the absolute value of the 2D Fourier map at ω_{T_w} = 264 cm^{-1}. The spectrum is dominated by four peaks, and each peak represents an intensity beating at the corresponding region of the 2D spectrum. A clear demarcation into four peaks is an indication of the phase difference among them, which is also observed in the kinetic traces in Fig. 4. The pattern of the 2D Fourier maps [Fig. 5(a)] is consistent with the nature of the CLS beating. The beating in CLS arises

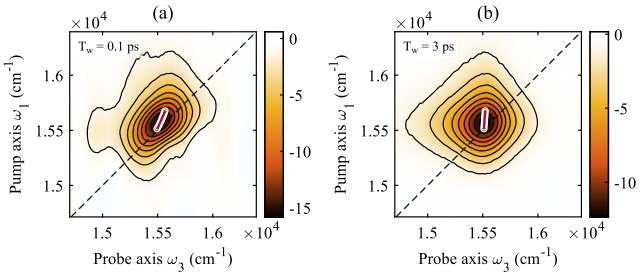

FIG. 2. 2D electronic spectra measured with setup I at 0.1 ps (a) and 3 ps (b) overlaid with the CLSω_3 analysis result. The center points are plotted as white circles, and the fit center lines are dark red.

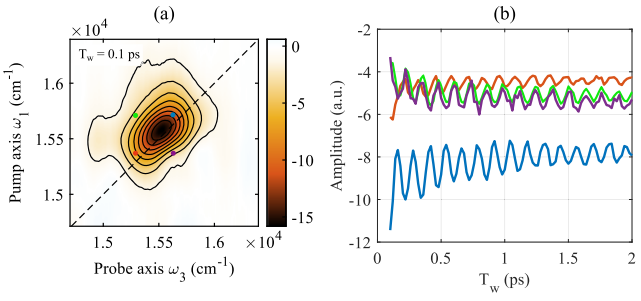

FIG. 4. (a) 2D spectrum at T_w = 0.1 ps of the 0–0 vibronic diagonal peak and (b) kinetic traces at the diagonal (blue and red) and anti-diagonal (purple and green) regimes.

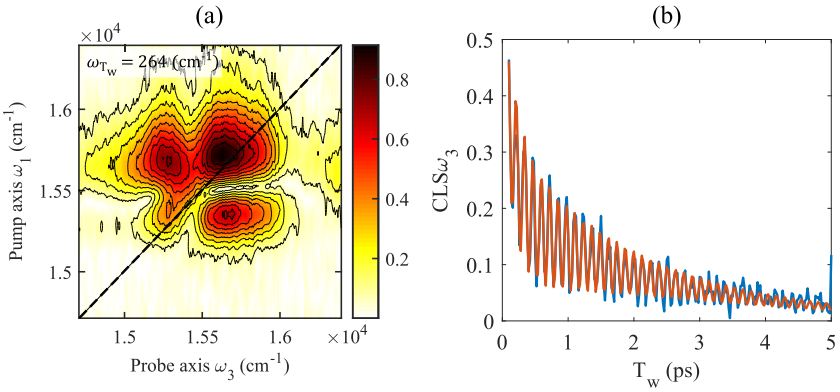

FIG. 5. (a) 2D Fourier map of the 0–0 vibronic diagonal peak at ω_{T_w} = 264 cm^{-1}. (b) Experimental CLSω_3 value (blue) of the diagonal peak and corresponding fit result (red).

from periodic variation in the peak shape akin to a rocking boat. This motion manifests itself as the points near the diagonal (blue and red) oscillate out-of-phase with the points on the anti-diagonal (purple and green) in Fig. 4(a). CLS analysis is a method of quantifying the change in peak shape over time, and the oscillation of the CLS value is associated with the amplitude beating.

Based on the measured CLSω_3, we obtained the normalized FFCF of the 0–0 vibronic diagonal peak. The CLSω_3 kinetics can be fit well with a function that consists of two exponential decays and one damped oscillatory function as follows:

$$CLS\omega_3(T_w) = a_1 \exp\left(-\frac{T_w}{\tau_1}\right) + a_2 \exp\left(-\frac{T_w}{\tau_2}\right) + a_v \exp\left(-\frac{T_w}{\tau_v}\right)\cos(\omega_v T_w + n\pi). \quad (8)$$

The results of the fit are presented in Fig. 5(b) and Table I. In this fit, τ_1 and τ_2 can be interpreted as the correlation times of the bath, and τ_v is the coherence time of the vibrational mode ω_v.

Based on the displaced harmonic oscillator model presented in the Theory section, we simulate the CLSω_3 values of the 0–0 vibronic transition. We used Eqs. (1)–(4) to calculate the response functions of the nonrephasing and rephasing processes and to generate the absorptive 2D electronic spectra in the impulsive limit.[16] The lineshape function used is discussed in the section Theory as contributions from a bath and a vibration mode representing the oscillations [Eqs. (5)–(7)]. The parameters used to calculate the lineshape function are presented in Table II.

From the simulated 2D electronic spectra, CLSω_3 analysis was performed [Figs. 6(a) and 6(b)] and the result is plotted in comparison with the experimental data [Fig. 6(c)]. The parameters in Table II are chosen according to the following reasons. For the bath components, the inverse correlation time γ_k in Table II are taken as the inverse of the value of τ_k (k = 1, 2) in Table I. For the vibrational component, the frequency ω_v and the damping rate γ_v in Table II are used based on ω_v and τ_v in Table I, respectively. The fluctuation amplitudes Δ_k are scaled up from the a_k values, with a factor that takes into consideration, together with a homogeneous dephasing time T_2, to fit the linear spectrum and the decay dynamics of the measured CLSω_3. This is done while keeping the relative values of Δ_k the same as the relative values of a_k. The temperature used in the simulation is 300 K. From Figs. S2a and S2b, it can be seen that the calculated absorption spectrum and the CLSω_3 decay dynamics fit well with the experimental data. Finally, the reorganization energy of the vibrational mode λ_v is then adjusted to fit the oscillation amplitude of the CLSω_3 value. Adding an extra high frequency mode, such as the ~1300 cm^{-1} mode, into the simulation introduces only a minimal change in the calculated absorption spectrum and 2D peak shape of the 0–0 vibronic transition. Details are available in the supplementary material (Sec. 4).

Excitation of the 0–1 transition (setup II)

2DES data were also collected for solution of TIPS-Pn with higher T_w resolution and larger bandwidth using setup II. Data were initially collected in toluene. However, it was found that strong

TABLE I. The fitting result for the CLSω_3.

a_1	a_2	a_v	$\tau_1(ps^{-1})$	$\tau_2(ps^{-1})$	$\tau_v(ps^{-1})$	$\omega_v(cm^{-1})$	n
0.34 ± 0.06	0.18 ± 0.03	0.16 ± 0.04	0.18 ± 0.05	3.00 ± 0.41	2.24 ± 0.02	257.9 ± 0.1	0.68 ± 0.07

TABLE II. The parameters of the lineshape function $g(t)$ used in the simulation.

$T_2(ps)$	Δ_1^2 (ps^{-2})	Δ_2^2 (ps^{-2})	$\gamma_1(ps^{-1})$	$\gamma_2(ps^{-1})$	$\omega_v(cm^{-1})$	$\gamma_v(ps^{-1})$	$\lambda_v(cm^{-1})$
0.05	468.6	243.7	5.55	0.33	257.9	0.455	26

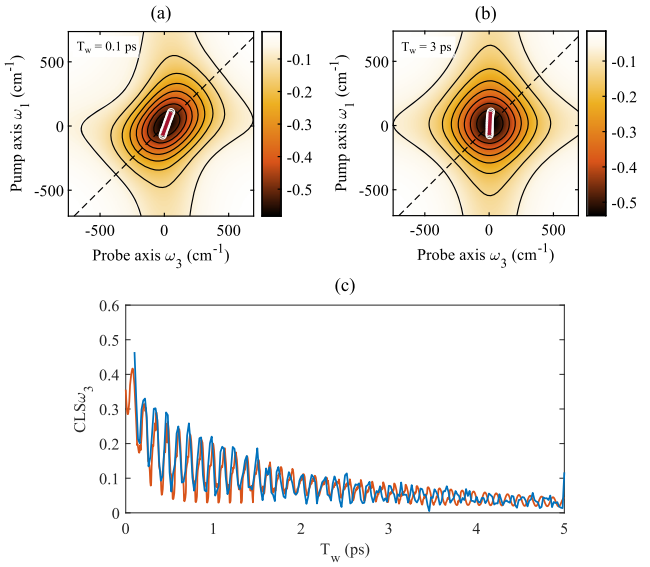

FIG. 6. The simulated 2D electronic spectra at T_w = 0.1 ps (a) and 3 ps (b) presented in the same fashion as Fig. 2. (c) The experimental CLSω_3 of the diagonal peak (blue) in comparison with the CLSω_3 calculated from the simulation (red).

coherent signals attributed to toluene around 800 and 1050 cm^{-1} obscured potential TIPS-Pn coherence. THF was chosen as the alternative solvent because the frequencies of its coherent signal were found to overlap minimally with those of TIPS-Pn. Distilling the THF prior to use reduces the concentration of dissolved oxygen and hence reduces degradation of the TIPS-Pn by photooxidation.[54]

The larger bandwidth allowed observation of the diagonal peaks corresponding to GSB and SE of both the 0–1 transition and partially the 0–0 transition [Fig. 7(a)], respectively. The off-diagonal peak, which corresponds to the excitation of the 0–1 transition and detection at the 0–0 transition frequency, is strong, indicating rapid relaxation from the first to the ground vibrational state during the waiting time. At ω_3 = 17 300 cm^{-1}, the observed excited-state absorption (ESA) signals are attributed to absorbance from the first excited singlet state to higher singlet states.[40] Over the waiting time, this broad pattern of signals persists at similar intensity up to 500 fs [Fig. 7(b)], indicating that the population of singlet TIPS-Pn is unchanged. This result is consistent with the relatively long singlet lifetime (~13 ns) and lack of SF in a dilute solution. In addition, the data exhibit complex and long-lived oscillation at multiple frequencies [Fig. 7(b)].

As with the previous data from setup I, we analyzed these oscillatory features by Fourier transforming the 2D electronic spectrum over T_w, generating the third axis, ω_{T_w}. By integrating the resultant 2D Fourier maps over ω_1 and ω_3, oscillatory features with frequencies of 313, 940, and 1173 cm^{-1} are present, with additional weaker signals around 500 and 800 cm^{-1}. Because of the limit in the waiting time range, the error bar of the integrated value calculated from the 2D Fourier map is 80 cm^{-1} [estimated FWHM from Fig. 7(c)], and it is likely that these peaks are broadened due to this error bar. The integrated value of the Fourier transformed 2D spectra is somewhat noisy due to this relatively low spectral resolution and the presence of multiple signals with closely spaced frequencies. The 2D Fourier maps at 313 and 1173 cm^{-1} (Figs. 8 and 9), however, have a clear and distinct ω_1- and ω_3-dependence, indicating that these

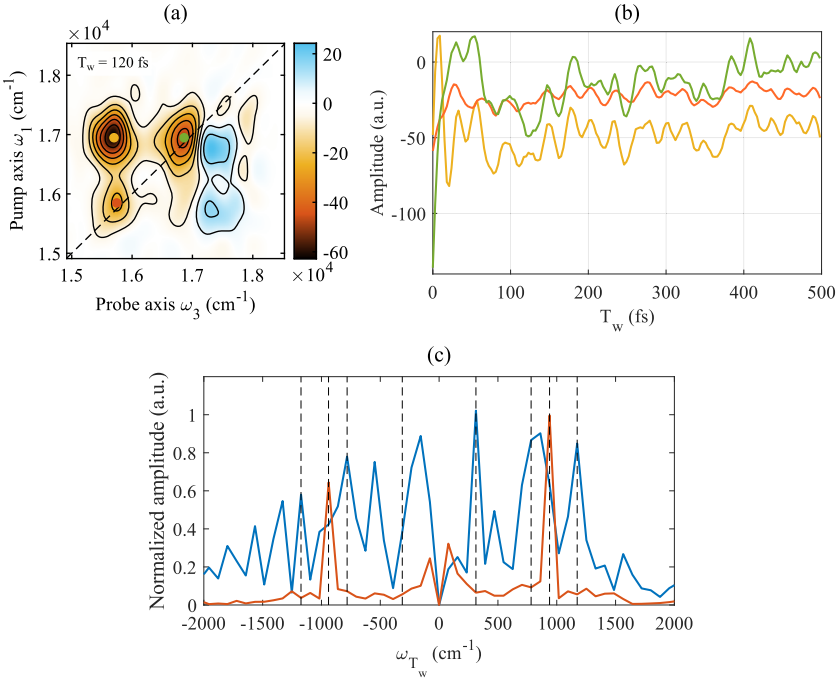

FIG. 7. (a) 2D electronic spectrum at T_w = 120 fs measured with setup II and (b) kinetic traces at the diagonal (red and green) and the anti-diagonal (yellow) regimes. (c) The integrated values of the Fourier transformed 2D spectra of TIPS-Pn (blue) and the solvent THF (red). The values presented are absolute values. The dashed lines indicate the relevant vibrational modes: ±313, ±788, ±940, and ±1173 cm^{-1}.

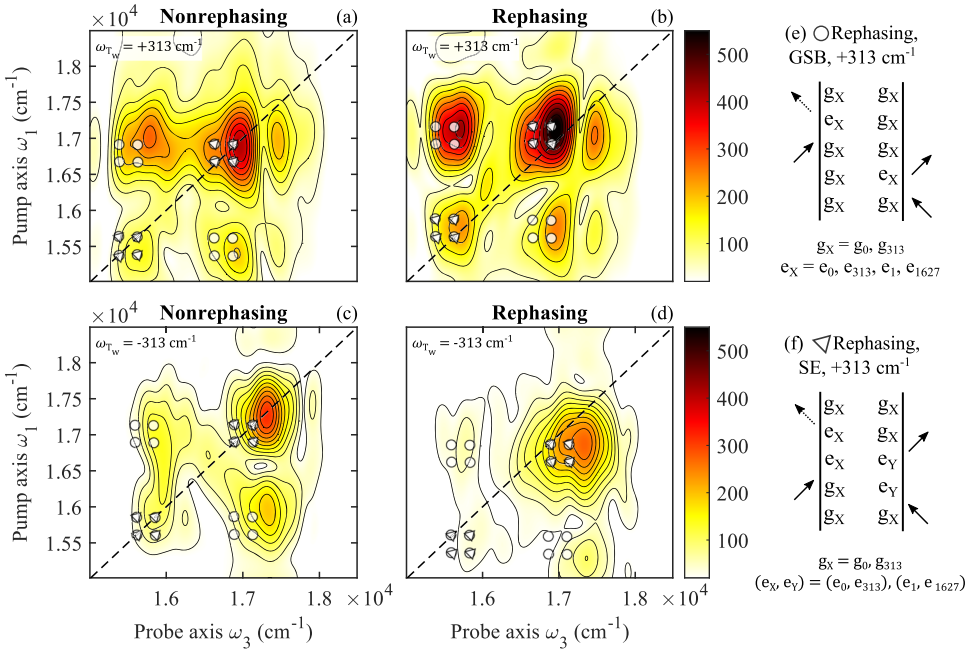

FIG. 8. 2D Fourier maps of the nonrephasing [(a) and (c)] and rephasing [(b) and (d)] at frequency $\omega_{T_w} = \pm 313$ cm^{-1}, with coherence locations based on the model described in the main text marked with circles (GSB) and triangles (SE). (e) and (f) DSFDs for the 2D Fourier maps (b) where g is denoted as the ground state, e is the excited state, and the subscripts are the corresponding vibrational frequency.

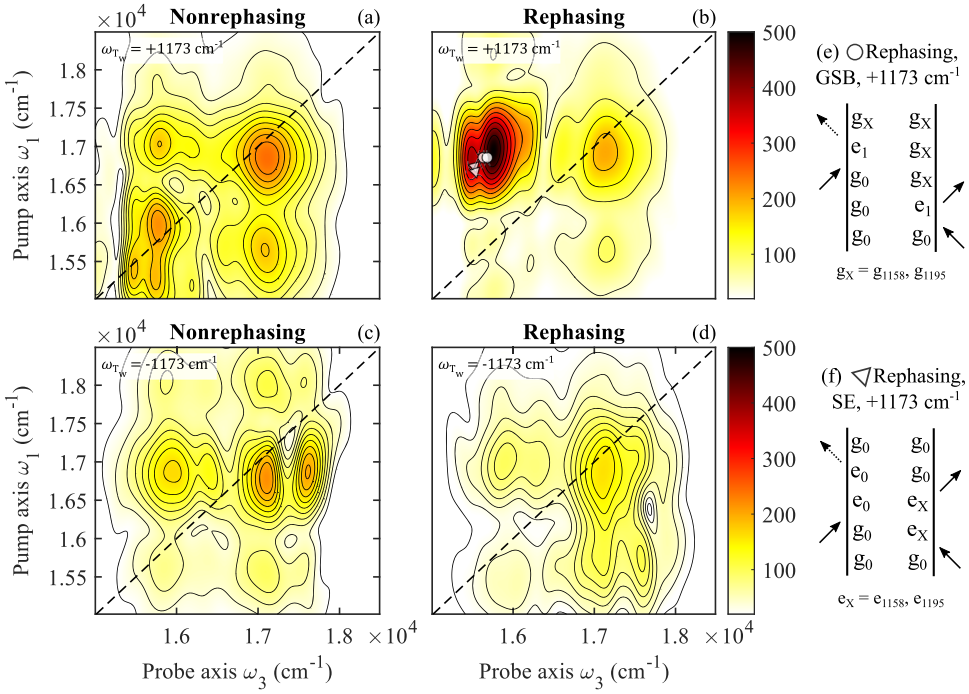

FIG. 9. 2D Fourier maps of the nonrephasing [(a) and (c)] and rephasing [(b) and (d)] at frequency $\omega_{T_w} = \pm 1173$ cm^{-1}. (e) and (f) DSFDs for the 2D Fourier map (b) with their predicted locations marked with white circles and triangles. The notations used here are similar to that in Fig. 8.

signals are distinguishable from noise and are likely to result from real coherence within the sample. Apart from the 940 cm^{-1} vibration, the frequencies are consistent with the Raman spectrum of TIPS-Pn (Fig. S5)[38,39,55] and are likely to result from coherence within the vibronic states of TIPS-Pn. The 940 cm^{-1} signal is consistent with a strong Raman mode of the solvent, THF.[56] To confirm this assignment, we collected data for a sample of THF without TIPS-Pn and found a strong coherent signal at 940 cm^{-1}. The 2D Fourier maps for this mode are similar in the presence and absence of TIPS-Pn (Figs. S3 and S4), indicating that this mode is attributed to a non-resonant response of the solvent THF.

To investigate the modes attributed to TIPS-Pn in more detail, we present the 2D Fourier maps at ω_{T_w} = ±313 and ±1173 cm^{-1} in Figs. 8 and 9, respectively. The BOXCARS geometry of setup II allows separation of the 2D Fourier maps into nonrephasing and rephasing maps and by the sign of ω_{T_w}, resulting in four distinct 2D Fourier maps. Since different subsets of DSFDs are contained in the four 2D Fourier maps, separating them can aid the characterization and assignment of the vibronic coherences.[57,58]

The absolute value of the four 2D Fourier maps for the low frequency mode ω_{T_w} = ±313 cm^{-1} is given in Fig. 8. Due to the low resolution of ω_{T_w}, these maps are likely to originate from the 264 cm^{-1} mode, which has been discussed in the section titled Excitation of the 0–0 transition (setup I). Each map has a distinct pattern of four signals, arranged in a square formation with the side length equal to the energy difference between the first and second vibronic states (~1300 cm^{-1}). Although the four 2D Fourier maps appear to be very similar, closer inspection reveals that for the nonrephasing maps, the diagonal peaks are localized directly on the diagonal, while the corresponding peaks in the rephasing maps are shifted above and below the diagonal, for the negative and positive ω_{T_w} maps, respectively, by an amount corresponding to a coherence frequency of 313 cm^{-1}. Additionally, some peaks in the 2D Fourier maps have a diffuse, somewhat square shape [Fig. 8(b)], indicating the presence of multiple coherence pathways with slightly different ω_1 and ω_3. In addition to the observed 313 cm^{-1} mode, we observed high-frequency coherences at ω_{T_w} = ±788 and ±1173 cm^{-1}. The 2D Fourier maps for the 788 cm^{-1} mode are particularly noisy and diffuse, prohibiting confident assignment by DSFDs. The 2D Fourier maps for the higher frequency mode, ±1173 cm^{-1}, have stronger signals (Fig. 9) and can be analyzed more easily. DSFDs can be used to rationalize the appearance of the 2D Fourier maps at frequency ±313 and ±1173 cm^{-1} and will be provided in the Discussion section.

DISCUSSION

Setup I revealed much information regarding the lineshape function of the 0–0 vibronic transition. The most striking feature observed in the 2D electronic spectrum of TIPS-Pn is the intense oscillation observed in both the CLSω_3 and the amplitude of the diagonal peak. All the observed beating has a frequency of 264 ± 8 cm^{-1}. The published vibrational spectrum of pentacene, a molecule similar to TIPS-Pn with its five-benzene ring skeleton, shows a band at 264 cm^{-1}, which was assigned to the ring-breathing mode of the molecule.[50] The Raman spectrum of TIPS-Pn (Fig. S6) and DFT calculation (Fig. S7a) also shows a peak at 264 cm^{-1} and similar assignment on the motion of the vibration. In view of the assignment, we can rationalize the strong coupling between the vibrational and electronic degrees of freedom (parameterized by the Huang–Rhys factor). In a π-conjugated system, there is often a strong coupling between the geometric and electronic structure.[59] When a vibrational mode strongly affects the geometry of the π-conjugated system, it modulates the HOMO–LUMO energy gaps. In this case, the mode is the ring-breathing mode, which stretches the TIPS-Pn molecule in the horizontal direction along the conjugated system (Fig. S7a). The sinusoidal modulation of the HOMO–LUMO energy gap manifests itself as a beating observed in the normalized FFCF and the 2D signal amplitude.

Another feature obtained from CLS analysis is the spectral diffusion dynamics. By fitting the CLSω_3 with a sum of exponential decays and a damped oscillatory function [see Eq. (8) and Fig. 5(b)], we resolved two spectral diffusion lifetimes. The first lifetime, τ_1 of 180 fs, can be assigned to the inertial component of solvation arising from the librational motion of the solvent molecules.[60] The second lifetime, τ_2 of 3 ps, can be assigned to diffusive dynamics of solvent molecules.[60] Numerous studies performed on various solvents uncovered both the fast dynamics in the time range of sub-ps[27,47,61] and the slow dynamics in the range of several to tens of ps dynamics.[62,63] We also note that we did not observe any substantial dynamics at T_w > 10 ps timescale, which are usually ascribed to various intermolecular interactions.[27,28,64] Some molecular systems exhibit spectral diffusion dynamics at this slow timescale (tens to hundreds of ps) due to stronger interactions with the solvents. Examples include chlorophyll-like systems that undergo hydrogen-bonding[27,64] or ligation dynamics between nucleophilic solvent molecules and the metal center of chlorophylls.[28] In the case of TIPS-Pn, the absence of a lifetime longer than 10 ps suggests that the optical transition of the molecule is likely insensitive to solvation dynamics of nonpolar solvents. In our study, there is also no constant offset or ns timescale decay, suggesting that there is negligible structural inhomogeneity in the system.[65,66] Structural inhomogeneity is often due to the chromophores having long chains, resulting in multiple possible conformers in the solvent environment. In the present case, TIPS-Pn, having a rigid fused five-membered aromatic ring structure, is not expected to exhibit multiple conformers.

Simulations were performed with the parameters obtained from the experimental CLSω_3 (see Table II), such as beating frequency, phase, decay lifetime, and amplitude. To obtain a reasonable fit to the observed oscillation amplitude [Fig. 6(c)], we used a vibrational reorganization energy of value λ_v = 26 cm^{-1} (which gives the Huang–Rhys factor a value of $S_v = \frac{\lambda_v}{\omega_v}$ = 0.1). The Huang–Rhys factor measures the strength of coupling between the vibrational and electronic degree of freedom[46] and has been calculated for multiple systems using various methods.[67–69] Our qualitative measure of the amplitude of the Huang–Rhys factor is comparable to those calculated from synthetic dye molecules.[70–72] Further refinement of the simulation can be carried out by more sophisticated fits, by, for example, including finite laser pulse effects,[73–75] and may allow us to obtain reliably the experimental values of the Huang–Rhys factor for the vibronic couplings.

Further studies by exciting and detecting at the 0–0 and 0–1 transition using setup II provided information regarding the coherence of different vibronic states as the pump pulse covered

a wider frequency range. We obtain the 2D Fourier maps at frequency $\omega_{T_w} = \pm 313$ cm^{-1}, which within the uncertainty of ±80 cm^{-1} (due to the limited range of the T_w window) can be assigned to the 264 cm^{-1} mode. We can use DSFDs to assign the coherence, assuming the vibrational mode is located in both the ground and first singlet excited states. Both GSB and SE diagrams can contribute to the observed coherence. For SE pathways, we assumed a minimal Stokes shift, as has been reported previously.[76] As an example, the DSFDs for the rephasing 2D Fourier map at $\omega_{T_w} = +313$ cm^{-1} are given in Figs. 8(e) and 8(f); the diagrams for the remaining maps are analogous. Initially, we found that the beating maps are reasonably well predicted by pathways utilizing transition from g_0 to e_0, e_1, and e_{313}. However, these pathways fail to account for the high energy coherence observed at region $(\omega_1, \omega_3) = (17\,200, 17\,200)$ cm^{-1}. To account for these signals, we note that TIPS-Pn has a high frequency Raman mode at 1627 cm^{-1} (Fig. S6), which is 253 cm^{-1} above the strong 1374 cm^{-1} mode.[38] Coherence between these two states would give rise to an oscillation with frequency $\omega_{T_w} = 313 \pm 80$ cm^{-1} and hence appear on this low frequency beating map. Including pathways with coherence between these two states leads to better agreement with the beating maps. There may also be an additional contribution from ESA pathways in these 2D Fourier maps, indicated by the weak signal at $\omega_3 = 17\,300$ cm^{-1}, the energy of transition to higher singlet states. Similar assignments are done with the dominant rephasing 2D Fourier maps at $\omega_{T_w} = +1173$ cm^{-1} [Fig. 9(b)]. Due to the low resolution of the ω_{T_w} axis, these maps likely contain contributions from both the 1158 and 1195 cm^{-1} modes (Fig. S6). The 1158 cm^{-1} mode is the C–H bending of the outer rings, and the 1195 mode is the C–H bending with the ring twisting (Figs. S7c and S7d). Both GSB and SE pathways were found to match the observed coherence, indicating that this mode may be present in both the ground and first singlet excited states. Overall, analysis of the coherence of TIPS-Pn measured using setup II reveals vibrational coherence at frequencies consistent with the Raman modes of TIPS-Pn. Assignment by DSFDs found that both GSB and SE pathways are consistent with the ω_1- and ω_3-dependence of the coherence, indicating that the vibronic structure of the first singlet state is likely to be the same as the ground state.

The modes analyzed above are consistent with those observed by Musser *et al.*[38] and Bakulin *et al.*[39] for thin films of polycrystalline TIPS-Pn, where SF is rapid and hence the system has a significant population of triplet excited states. Bakulin *et al.*[39] also highlighted the existence of a 264 cm^{-1} vibronic state in the triplet pair manifold; this state is nearly in resonance with the lowest excited singlet state and maybe involved in ultrafast SF in TIPS-Pn. The coherence reported here of TIPS-Pn in diluted solution in the absence of SF serves as an important control study for 2DES experiment on crystalline TIPS-Pn and aids with disentangling vibronic coherence associated with the singlet and triplet states of TIPS-Pn.

CONCLUSIONS

In summary, we measured and analyzed 2D electronic spectra of TIPS-Pn in solution. Using setup I, we obtained 2DES data for the 0–0 vibronic transition. Detailed analyses of these data revealed for the first time an intense oscillatory feature of CLSω_3 over the waiting time with a frequency of 264 ± 8 cm^{-1}. Furthermore, the amplitude beating of 2D spectra showed similar oscillation frequency with the beating pattern consistent with the nature of the CLS beating. Based on previous studies, this mode has been assigned to the pentacene ring-breathing vibrational mode. We concluded that the beating observed in both the spectral amplitude and the CLS value is due to the strong modulation this vibrational mode exerts on the HOMO–LUMO gap of TIPS-Pn through the geometric change. In addition, the CLS data allowed us to extract solvation dynamics, as well as the beating dynamics. We used the displaced harmonic oscillator model to simulate the 2D electronic spectra and CLSω_3 value. A Huang–Rhys factor of 0.1 was used to generate the 2D electronic spectrum, and the subsequent analysis provided strong concurrence with our experimental data, which indicates the validity of this model. The assignment of this mode as the ring-breathing vibrational mode, which is expected to have a periodic perturbation on the transition frequency, is also consistent with the observation. From setup II, we obtained information regarding the coherence between different vibrational modes of the molecule. The vibration around 264 cm^{-1} was again observed in diagonal and cross peaks near the 0–0 and 0–1 transitions of TIPS-Pn. The appearance of the 2D Fourier maps for this mode were rationalized by DSFDs assignment, with the 264 cm^{-1} mode presente in both the ground and first excited singlet states. Additional higher frequency vibrations consistent with the Raman modes of TIPS-Pn belonging to C–H bending of the outer rings and the C–H bending with the ring twisting were also observed, indicating that in the absence of SF, TIPS-Pn displays strong vibrational and vibronic coherence within the singlet states.

SUPPLEMENTARY MATERIAL

The supplementary material contains details on (1) lineshape function derivation based on the displaced harmonic oscillator model; (2) CLS analysis of the diagonal peak; (3) global analysis and beating map retrieval; (4) simulation of 2DES and CLS value, and 2D Fourier maps of THF in the presence and absence of TIPS-Pn; and (5) Raman spectrum and Raman mode assignment of TIPS-Pn.

ACKNOWLEDGMENTS

H.-S.T. acknowledges support from the Singapore Ministry of Education Academic Research Fund (Grant No. Tier 1 RG2/19). J.M.d.l.P. was supported by an Australian Government Research Training Program (RTP) scholarship. T.W.K. and G.D.S. acknowledge funding from the Australian Research Council (Grant Nos. DP160103797, LE0989747, and LE130100158).

DATA AVAILABILITY

The data that support the findings of this study are available from the corresponding authors upon reasonable request.

REFERENCES

[1]M. Sliwa, N. Mouton, C. Ruckebusch, S. Aloïse, O. Poizat, G. Buntinx, R. Métivier, K. Nakatani, H. Masuhara, and T. Asahi, "Comparative investigation of ultrafast photoinduced processes in salicylidene-aminopyridine in solution and solid state," J. Phys. Chem. C **113**, 11959–11968 (2009).

[2]E. Vella, H. Li, P. Grégoire, S. M. Tuladhar, M. S. Vezie, S. Few, C. M. Bazán, J. Nelson, C. Silva-Acuña, and E. R. Bittner, "Ultrafast decoherence dynamics

govern photocarrier generation efficiencies in polymer solar cells," Sci. Rep. **6**, 29437 (2016).
[3]P. Akhtar, C. Zhang, T. N. Do, G. Garab, P. H. Lambrev, and H.-S. Tan, "Two-dimensional spectroscopy of chlorophyll a excited-state equilibration in light-harvesting complex II," J. Phys. Chem. Lett. **8**, 257–263 (2017).
[4]F. D. Fuller and J. P. Ogilvie, "Experimental implementations of two-dimensional Fourier transform electronic spectroscopy," Annu. Rev. Phys. Chem. **66**, 667–690 (2015).
[5]K. L. M. Lewis and J. P. Ogilvie, "Probing photosynthetic energy and charge transfer with two-dimensional electronic spectroscopy," J. Phys. Chem. Lett. **3**, 503–510 (2012).
[6]P. D. Dahlberg, A. F. Fidler, J. R. Caram, P. D. Long, and G. S. Engel, "Energy transfer observed in live cells using two-dimensional electronic spectroscopy," J. Phys. Chem. Lett. **4**, 3636–3640 (2013).
[7]P. Malý, J. M. Gruber, R. J. Cogdell, T. Mančal, and R. van Grondelle, "Ultrafast energy relaxation in single light-harvesting complexes," Proc. Natl. Acad. Sci. U. S. A. **113**, 2934–2939 (2016).
[8]T. Stoll, E. Sgrò, J. W. Jarrett, J. Réhault, A. Oriana, L. Sala, F. Branchi, G. Cerullo, and K. L. Knappenberger, "Superatom state-resolved dynamics of the $Au_{25}(SC_8H_9)_{18}^-$ cluster from two-dimensional electronic spectroscopy," J. Am. Chem. Soc. **138**, 1788–1791 (2016).
[9]J. W. Jarrett, C. Yi, T. Stoll, J. Rehault, A. Oriana, F. Branchi, G. Cerullo, and K. L. Knappenberger, "Dissecting charge relaxation pathways in CdSe/CdS nanocrystals using femtosecond two-dimensional electronic spectroscopy," Nanoscale **9**, 4572–4577 (2017).
[10]E. Romero, R. Augulis, V. I. Novoderezhkin, M. Ferretti, J. Thieme, D. Zigmantas, and R. van Grondelle, "Quantum coherence in photosynthesis for efficient solar energy conversion," Nat. Phys. **10**, 676–682 (2014).
[11]E. Collini, H. Gattuso, L. Bolzonello, A. Casotto, A. Volpato, C. N. Dibenedetto, E. Fanizza, M. Striccoli, and F. Remacle, "Quantum phenomena in nanomaterials: Coherent superpositions of fine structure states in CdSe nanocrystals at room temperature," J. Phys. Chem. C **123**, 31286–31293 (2019).
[12]H. Seiler, S. Palato, C. Sonnichsen, H. Baker, E. Socie, D. P. Strandell, and P. Kambhampati, "Two-dimensional electronic spectroscopy reveals liquid-like lineshape dynamics in $CsPbI_3$ perovskite nanocrystals," Nat. Commun. **10**, 4962 (2019).
[13]S. Takahashi and K. Watanabe, "Decoupling from a thermal bath via molecular polariton formation," J. Phys. Chem. Lett. **11**, 1349–1356 (2020).
[14]M. Cho, H. M. Vaswani, T. Brixner, J. Stenger, and G. R. Fleming, "Exciton analysis in 2D electronic spectroscopy," J. Phys. Chem. B **109**, 10542–10556 (2005).
[15]E. L. Read, G. S. Engel, T. R. Calhoun, T. Mancal, T. K. Ahn, R. E. Blankenship, and G. R. Fleming, "Cross-peak-specific two-dimensional electronic spectroscopy," Proc. Natl. Acad. Sci. U. S. A. **104**, 14203–14208 (2007).
[16]P. Hamm and M. Zanni, *Concepts and Methods of 2D Infrared Spectroscopy* (Cambridge University Press, Cambridge, 2011).
[17]O. Rancova, R. Jankowiak, and D. Abramavicius, "Probing environment fluctuations by two-dimensional electronic spectroscopy of molecular systems at temperatures below 5 K," J. Chem. Phys. **142**, 212428 (2015).
[18]E. E. Fenn and M. D. Fayer, "Extracting 2D IR frequency-frequency correlation functions from two component systems," J. Chem. Phys. **135**, 074502 (2011).
[19]D. G. Osborne and K. J. Kubarych, "Rapid and accurate measurement of the frequency-frequency correlation function," J. Phys. Chem. A **117**, 5891–5898 (2013).
[20]J. D. Hybl, A. Yu, D. A. Farrow, and D. M. Jonas, "Polar solvation dynamics in the femtosecond evolution of two-dimensional Fourier transform spectra," J. Phys. Chem. A **106**, 7651–7654 (2002).
[21]T. Brixner, T. Mančal, I. V. Stiopkin, and G. R. Fleming, "Phase-stabilized two-dimensional electronic spectroscopy," J. Chem. Phys. **121**, 4221–4236 (2004).
[22]M. Cho, J.-Y. Yu, T. Joo, Y. Nagasawa, S. A. Passino, and G. R. Fleming, "The integrated photon echo and solvation dynamics," J. Phys. Chem. **100**, 11944–11953 (1996).
[23]X. Leng, T. N. Do, P. Akhtar, H. L. Nguyen, P. H. Lambrev, and H. S. Tan, "Hierarchical equations of motion simulation of temperature-dependent two-dimensional electronic spectroscopy of the chlorophyll a manifold in LHCII," Chem. - Asian J. **15**, 1996–2004 (2020).
[24]S. T. Roberts, J. J. Loparo, and A. Tokmakoff, "Characterization of spectral diffusion from two-dimensional line shapes," J. Chem. Phys. **125**, 084502 (2006).
[25]K. Kwak, S. Park, I. J. Finkelstein, and M. D. Fayer, "Frequency-frequency correlation functions and apodization in two-dimensional infrared vibrational echo spectroscopy: A new approach," J. Chem. Phys. **127**, 124503 (2007).
[26]K. L. Wells, Z. Zhang, J. R. Rouxel, and H.-S. Tan, "Measuring the spectral diffusion of chlorophyll a using two-dimensional electronic spectroscopy," J. Phys. Chem. B **117**, 2294–2299 (2013).
[27]M. F. Khyasudeen, P. J. Nowakowski, H. L. Nguyen, J. H. N. Sim, T. N. Do, and H.-S. Tan, "Studying the spectral diffusion dynamics of chlorophyll a and chlorophyll b using two-dimensional electronic spectroscopy," Chem. Phys. **527**, 110480 (2019).
[28]T. N. Do, J. H. N. Sim, H. L. Nguyen, Y. Lu, and H.-S. Tan, "Observing the fluctuation dynamics of dative bonds using two-dimensional electronic spectroscopy," J. Phys. Chem. Lett. **12**, 165–170 (2021).
[29]J. R. Caram, H. Zheng, P. D. Dahlberg, B. S. Rolczynski, G. B. Griffin, D. S. Dolzhnikov, D. V. Talapin, and G. S. Engel, "Exploring size and state dynamics in CdSe quantum dots using two-dimensional electronic spectroscopy," J. Chem. Phys. **140**, 084701 (2014).
[30]S. Bagchi, S. G. Boxer, and M. D. Fayer, "Ribonuclease S dynamics measured using a nitrile label with 2D IR vibrational echo spectroscopy," J. Phys. Chem. B **116**, 4034–4042 (2012).
[31]E. E. Fenn, D. B. Wong, C. H. Giammanco, and M. D. Fayer, "Dynamics of water at the interface in reverse micelles: Measurements of spectral diffusion with two-dimensional infrared vibrational echoes," J. Phys. Chem. B **115**, 11658–11670 (2011).
[32]A. Nemeth, F. Milota, T. Mančal, V. Lukeš, J. Hauer, H. F. Kauffmann, and J. Sperling, "Vibrational wave packet induced oscillations in two-dimensional electronic spectra. I. Experiments," J. Chem. Phys. **132**, 184514 (2010).
[33]F. Sanda, V. Perlik, C. N. Lincoln, and J. Hauer, "Center line slope analysis in two-dimensional electronic spectroscopy," J. Phys. Chem. A **119**, 10893–10909 (2015).
[34]M. J. Y. Tayebjee, K. N. Schwarz, R. W. MacQueen, M. Dvořák, A. W. C. Lam, K. P. Ghiggino, D. R. McCamey, T. W. Schmidt, and G. J. Conibeer, "Morphological evolution and singlet fission in aqueous suspensions of TIPS-pentacene nanoparticles," J. Phys. Chem. C **120**, 157–165 (2016).
[35]J. R. Allardice, A. Thampi, S. Dowland, J. Xiao, V. Gray, Z. Zhang, P. Budden, A. J. Petty II, N. J. L. K. Davis, N. C. Greenham, J. E. Anthony, and A. Rao, "Engineering molecular ligand shells on quantum dots for quantitative harvesting of triplet excitons generated by singlet fission," J. Am. Chem. Soc. **141**, 12907–12915 (2019).
[36]M. B. Smith and J. Michl, "Singlet fission," Chem. Rev. **110**, 6891–6936 (2010).
[37]M. B. Smith and J. Michl, "Recent advances in singlet fission," Annu. Rev. Phys. Chem. **64**, 361–386 (2013).
[38]A. J. Musser, M. Liebel, C. Schnedermann, T. Wende, T. B. Kehoe, A. Rao, and P. Kukura, "Evidence for conical intersection dynamics mediating ultrafast singlet exciton fission," Nat. Phys. **11**, 352–357 (2015).
[39]A. A. Bakulin, S. E. Morgan, T. B. Kehoe, M. W. B. Wilson, A. W. Chin, D. Zigmantas, D. Egorova, and A. Rao, "Real-time observation of multiexcitonic states in ultrafast singlet fission using coherent 2D electronic spectroscopy," Nat. Chem. **8**, 16–23 (2016).
[40]B. J. Walker, A. J. Musser, D. Beljonne, and R. H. Friend, "Singlet exciton fission in solution," Nat. Chem. **5**, 1019–1024 (2013).
[41]F. V. A. Camargo, H. L. Anderson, S. R. Meech, and I. A. Heisler, "Full characterization of vibrational coherence in a porphyrin chromophore by two-dimensional electronic spectroscopy," J. Phys. Chem. A **119**, 95–101 (2015).
[42]S. M. Hart, W. J. Chen, J. L. Banal, W. P. Bricker, A. Dodin, L. Markova, Y. Vyborna, A. P. Willard, R. Häner, M. Bathe, and G. S. Schlau-Cohen, "Engineering couplings for exciton transport using synthetic DNA scaffolds," Chem **7**, 752–773 (2021).
[43]J. A. Myers, K. L. M. Lewis, P. F. Tekavec, and J. P. Ogilvie, "Two-color two-dimensional Fourier transform electronic spectroscopy with a pulse-shaper," Opt. Express **16**, 17420–17428 (2008).

[44]S. Yan and H.-S. Tan, "Phase cycling schemes for two-dimensional optical spectroscopy with a pump–probe beam geometry," Chem. Phys. **360**, 110–115 (2009).
[45]P. C. Tapping, Y. Song, Y. Kobayashi, G. D. Scholes, and T. W. Kee, "Two-dimensional electronic spectroscopy using rotating optical flats," J. Phys. Chem. A **124**, 1053–1061 (2020).
[46]S. Mukamel, *Principles of Nonlinear Optical Spectroscopy* (Oxford University Press, Inc, 1995).
[47]S. A. Passino, Y. Nagasawa, T. Joo, and G. R. Fleming, "Three-pulse echo peak shift studies of polar solvation dynamics," J. Phys. Chem. A **101**, 725–731 (1997).
[48]T. H. S. Bican, H. W. Schrötter, and V. M. Grošev, "The Raman spectrum of toluene vapour," J. Raman Spectrosc. **26**, 787–790 (1995).
[49]J. Kapitán, L. Hecht, and P. Bouř, "Raman spectral evidence of methyl rotation in liquid toluene," Phys. Chem. Chem. Phys. **10**, 1003–1008 (2008).
[50]L.-Y. Chiu, H.-L. Cheng, H.-Y. Wang, W.-Y. Chou, and F.-C. Tang, "Manipulating the ambipolar characteristics of pentacene-based field-effect transistors," J. Mater. Chem. C **2**, 1823 (2014).
[51]Y.-C. Cheng and G. R. Fleming, "Coherence quantum beats in two-dimensional electronic spectroscopy," J. Phys. Chem. A **112**, 4254–4260 (2008).
[52]K.-H. Song, M. Gu, M.-S. Kim, H.-J. Kwon, H. Rhee, H. Han, and M. Cho, "Quantum beats and phase shifts in two-dimensional electronic spectra of zinc naphthalocyanine monomer and aggregate," J. Phys. Chem. Lett. **6**, 4314–4318 (2015).
[53]E. Meneghin, D. Pedron, and E. Collini, "Characterization of the coherent dynamics of bacteriochlorophyll a in solution," Chem. Phys. **519**, 85–91 (2019).
[54]S. Dong, A. Ong, and C. Chi, "Photochemistry of various acene based molecules," J. Photochem. Photobiol., C **38**, 27–46 (2019).
[55]D. T. James, B. K. C. Kjellander, W. T. T. Smaal, G. H. Gelinck, C. Combe, I. McCulloch, R. Wilson, J. H. Burroughes, D. D. C. Bradley, and J.-S. Kim, "Thin-film morphology of inkjet-printed single-droplet organic transistors using polarized Raman spectroscopy: Effect of blending TIPS-pentacene with insulating polymer," ACS Nano **5**, 9824–9835 (2011).
[56]Y. Takasu, S. Matsumoto, Y. Fujii, and I. Nishio, "Raman study of the low temperature behavior of tetrahydrofuran molecule in the cage of clathrate hydrate," Chem. Phys. Lett. **627**, 39–43 (2015).
[57]V. Butkus, D. Zigmantas, L. Valkunas, and D. Abramavicius, "Vibrational vs. electronic coherences in 2D spectrum of molecular systems," Chem. Phys. Lett. **545**, 40–43 (2012).
[58]D. V. Le, X. Leng, and H.-S. Tan, "Regarding expressions of the oscillatory patterns in the 2D spectra of a displaced oscillator model," Chem. Phys. **546**, 111142 (2021).
[59]N. E. Gruhn, D. A. da Silva Filho, T. G. Bill, M. Malagoli, V. Coropceanu, A. Kahn, and J.-L. Brédas, "The vibrational reorganization energy in pentacene: Molecular influences on charge transport," J. Am. Chem. Soc. **124**, 7918–7919 (2002).
[60]S. J. Rosenthal, R. Jimenez, G. R. Fleming, P. V. Kumar, and M. Maroncelli, "Solvation dynamics in methanol: Experimental and molecular dynamics simulation studies," J. Mol. Liq. **60**, 25–56 (1994).
[61]M. L. Horng, J. A. Gardecki, A. Papazyan, and M. Maroncelli, "Subpicosecond measurements of polar solvation dynamics: Coumarin 153 revisited," J. Phys. Chem. **99**, 17311–17337 (1995).
[62]Y. Nagasawa, A. Watanabe, H. Takikawa, and T. Okada, "Solute dependence of three pulse photon echo peak shift measurements in methanol solution," J. Phys. Chem. A **107**, 632–641 (2003).
[63]S. K. Karthick Kumar, A. Tamimi, and M. D. Fayer, "Comparisons of 2D IR measured spectral diffusion in rotating frames using pulse shaping and in the stationary frame using the standard method," J. Chem. Phys. **137**, 184201 (2012).
[64]R. Moca, S. R. Meech, and I. A. Heisler, "Two-dimensional electronic spectroscopy of chlorophyll a: Solvent dependent spectral evolution," J. Phys. Chem. B **119**, 8623–8630 (2015).
[65]S.-H. Lee, J.-H. Lee, and T. Joo, "Deuterium isotope effect on the solvation dynamics of a dye molecule in methanol and acetonitrile," J. Chem. Phys. **110**, 10969–10977 (1999).
[66]S. Park and T. Joo, "Diffractive optics based three-pulse photon echo peak shift studies of spectral diffusion in polar liquids: Evidence for long lived frequency correlations," J. Chem. Phys. **131**, 164508 (2009).
[67]T.-w. Huang, L. Yang, C. Zhu, and S. H. Lin, "Absorption and fluorescence spectra of the neutral and anionic green fluorescent protein chromophore: Franck–Condon simulation," Chem. Phys. Lett. **541**, 110–116 (2012).
[68]Y. Jing, R. Zheng, H.-X. Li, and Q. Shi, "Theoretical study of the electronic-vibrational coupling in the Q(y) states of the photosynthetic reaction center in purple bacteria," J. Phys. Chem. B **116**, 1164–1171 (2012).
[69]S. Skandary, M. Hussels, A. Konrad, T. Renger, F. Müh, M. Bommer, A. Zouni, A. J. Meixner, and M. Brecht, "Variation of exciton-vibrational coupling in photosystem II core complexes from Thermosynechococcus elongatus as revealed by single-molecule spectroscopy," J. Phys. Chem. B **119**, 4203–4210 (2015).
[70]T. Mančal, O. Bixner, N. Christensson, J. Hauer, F. Milota, A. Nemeth, J. Sperling, and H. F. Kauffmann, "Dynamics of quantum wave packets in complex molecules traced by 2D coherent electronic correlation spectroscopy," Procedia Chem. **3**, 105–117 (2011).
[71]S. H. Sohail, J. P. Otto, P. D. Cunningham, Y. C. Kim, R. E. Wood, M. A. Allodi, J. S. Higgins, J. S. Melinger, and G. S. Engel, "DNA scaffold supports long-lived vibronic coherence in an indodicarbocyanine (Cy5) dimer," Chem. Sci. **11**, 8546–8557 (2020).
[72]J. R. Caram, A. F. Fidler, and G. S. Engel, "Excited and ground state vibrational dynamics revealed by two-dimensional electronic spectroscopy," J. Chem. Phys. **137**, 024507 (2012).
[73]T. N. Do, M. F. Gelin, and H.-S. Tan, "Simplified expressions that incorporate finite pulse effects into coherent two-dimensional optical spectra," J. Chem. Phys. **147**, 144103 (2017).
[74]V. Perlík, J. Hauer, and F. Šanda, "Finite pulse effects in single and double quantum spectroscopies," J. Opt. Soc. Am. B **34**, 430–439 (2017).
[75]C. L. Smallwood, T. M. Autry, and S. T. Cundiff, "Analytical solutions to the finite-pulse Bloch model for multidimensional coherent spectroscopy," J. Opt. Soc. Am. B **34**, 419 (2017).
[76]A. D. Platt, J. Day, S. Subramanian, J. E. Anthony, and O. Ostroverkhova, "Optical, fluorescent, and (Photo)conductive properties of high-performance functionalized pentacene and anthradithiophene derivatives," J. Phys. Chem. C **113**, 14006–14014 (2009).